IEEE Photonics Journal
An IEEE Photonics Society Publication

Open Access

A Multi-Channel Multi-Bit Programmable Photonic Beamformer Based on Cascaded DWDM

Volume 6, Number 4, August 2014

Anliang Yu
Weiwen Zou, Senior Member, IEEE
Shuguang Li
Jianping Chen

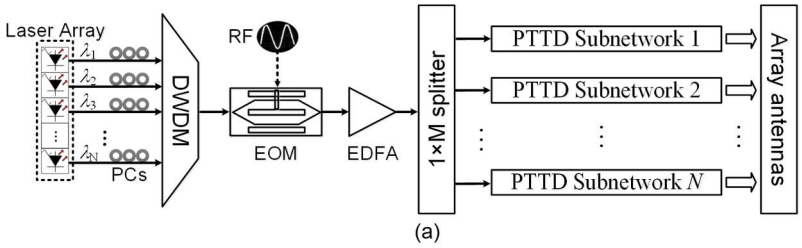

(a)

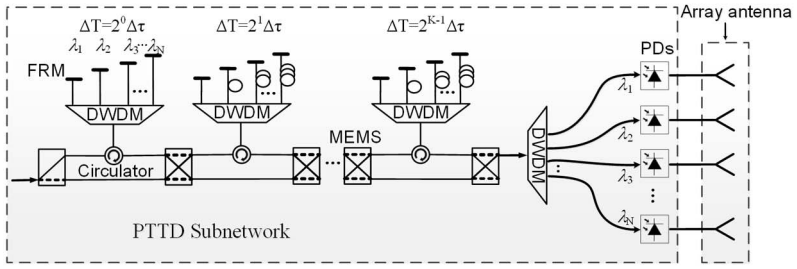

(b)

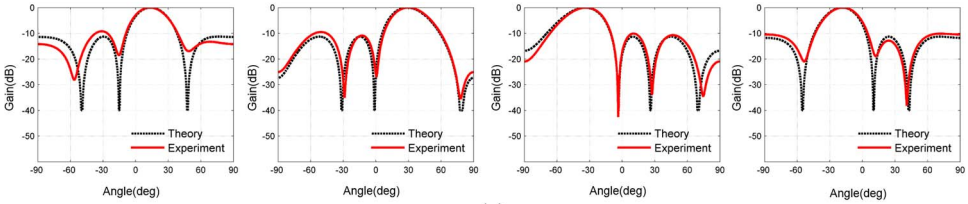

(c)

DOI: 10.1109/JPHOT.2014.2344007
1943-0655 © 2014 IEEE

A Multi-Channel Multi-Bit Programmable Photonic Beamformer Based on Cascaded DWDM

Anliang Yu,[1] Weiwen Zou,[1] *Senior Member, IEEE*, Shuguang Li,[2] and Jianping Chen[1]

[1]State Key Laboratory of Advanced Optical Communication Systems and Networks, Department of Electronic Engineering, Shanghai Jiao Tong University, Shanghai 200240, China
[2]Shanghai Aerospace Electronic Technology Institute, Shanghai 201109, China

DOI: 10.1109/JPHOT.2014.2344007

Manuscript received June 20, 2014; revised July 20, 2014; accepted July 22, 2014. Date of publication July 29, 2014; date of current version August 14, 2014. This work was supported in part by the 973 Program under Grant 2011CB301700; by the National Natural Science Foundation of China under Grants 61007052 and 61127016; by the Joint Project between Shanghai Jiao Tong University and Shanghai Academy of Spaceflight Technology; by Shanghai Pujiang Program under Grant 12PJ1405600; and by the State Key Lab Project of Shanghai Jiao Tong University under Grant 2014ZZ03016. Corresponding author: W. Zou (e-mail: wzou@sjtu.edu.cn).

Abstract: We propose and experimentally demonstrate a novel multi-channel multi-bit programmable photonic beamformer, which consists of multiple parallel photonic true-time delay (PTTD) subnetworks based on cascaded DWDMs. Each PTTD subnetwork can provide multi-bit true-time delays (TTDs) for a multi-channel modulated RF signal of a phased array antenna (PAA) and operate over a wide RF range from 10 MHz to 12 GHz. The RF signal is modulated to a spectrally separated laser array combined by a DWDM to form a multi-channel spatially separated PAA. The multi-bit TTDs for scanning PAA angles are rapidly programmed by means of a control circuit of optical switches in the PTTD subnetwork. By using an optical splitter, multiple parallel PTTD subnetworks can be topologically configured out for a PAA with a large number of elements. The obtained radiation patterns demonstrate that the proof-of-concept experimental result agrees well with the theoretical analysis, verifying the feasibility of the proposed photonic beamformer.

Index Terms: Microwave photonics, photonic beamformer, true-time delay, dense wavelength division multiplexer, radiation pattern, phased array antenna.

1. Introduction

The phased array antenna (PAA) is widely used in multifunctional radars and wireless communications [1], [2], etc., because the beam steering can be easily scanned via phase-shifting the radio frequency (RF) signals instead of physically moving the antenna. However, the conventional electrical phase shifters in PAAs suffer the intrinsic shortage of narrow bandwidth, which results in the well-known beam squint phenomenon for broadband signals [3]. In order to solve the problem, the photonic true-time delay (PTTD) techniques, implementing the beamformer in optical domain, have been proposed [4]. They are able to improve the performance greatly due to the inherent advantages, such as large bandwidth, low transmission loss, small size, no electro-magnetic interference, and multi-beam capability [5], [6]. The photonic beamformer

utilizing the PTTD techniques has become a promising method for next-generation wideband radar system.

Up to date, various PTTD schemes have been proposed for photonic beamformers, including the application of high dispersion fibers [7]–[9], fiber grating [10], [11], fiber-optic delay line matrix [12], spatial light modulator [13], single sideband polarization modulation [14], integrated photonics [15], and wavelength division multiplexing (WDM) technique [16]–[18]. All of them offer distinct advantages and have drawbacks at the same time in terms of the achievable delay, flatness of the RF response, dynamic range, ease of control, and system simplicity. For example, dispersive fiber technique is quite competitive in power and space consumption [7]–[9] but the bandwidth of the transmission signal is limited by the power fading of the broadband RF signal caused by the group velocity dispersion [19]. Besides, its programmable PTTD is determined by the product of optical wavelength of a tunable laser and the dispersion value [9], [20]. Consequently, the resolution and dynamic range of the PTTD are both linearly related to the dispersion value so that high resolution and large range are contradictory. In comparison, dense wavelength division multiplexer (DWDM) based PTTD [16]–[18] uses optical multiplexer/demultiplexer (such as thin film filter based one) to achieve very large RF bandwidths with lower phase and amplitude distortions, which are two non-ignorable factors in photonic beamformer. One of the key issues is the limitation of channel number in commercially available DWDMs, which leads to the tradeoff relation between the minimum delay step and the maximum delay range.

In this paper, we propose and experimentally demonstrate a novel multi-channel multi-bit programmable photonic beamformer for PAA with a large number of elements. It consists of multiple parallel PTTD subnetworks based on cascaded DWDMs. A multi-channel laser array serves as a set of wavelength-separated optical carriers simultaneously for all parallel PTTD subnetworks. Each PTTD subnetwork with wavelength-dependent operation is comprised of cascaded DWDMs, micro-electromechanical systems (MEMS) based optical switches, optical circulators, Faraday rotator mirrors (FRMs), and precisely tailored optical fiber segments. Multiple ports of each DWDM are spatially separated and connected with individual optical carriers (wavelengths) so as to configure out multi-channel photonic beamformer. Multi-bit PTTD with large dynamic delay value is obtained by switching the MEMS optical switches, which are laid between two neighboring stages of DWDMs. The resolution of PTTD, i.e., the minimum delay step, is guaranteed by the precise fiber tailoring and measurement techniques [21], [22]. A proof-of-concept experiment is carried out to verify the radiation patterns of PAA, and the experimental result is in a good agreement with theoretical analysis.

2. Operating Principle

PAA technology requires fast and accurate beam pattern shaping and reconfiguring through the implementation of a beamformer, which can be generally defined as a beamforming network capable of generating the desired amplitude and phase excitations at each specific PAA element. In an evenly distributed linear PAA, the far-field array radiation pattern $(F(\theta))$ at a scanning angle θ is determined by the summation of the individual PAA elements as follows [23], [24]:

$$F(\theta) = \sum_{i=0}^{N-1} a_i \exp\left(j(ikd\sin\theta + \varphi_i)\right) \tag{1}$$

where N is the number of PAA elements, k $(= 2\pi/\lambda$ with λ the RF wavelength) is the wavenumber, and d $(= \lambda/2$ or $\lambda/4)$ is the spatial distance between the neighboring elements. a_i and φ_i represent the amplitude and phase excitations of the ith element, determining the characteristics of the formed beam pattern.

In PAA, the beam pattern is formed by exactly adjusting the phase difference between the adjacent antenna elements as $\Delta\phi_B = kd\sin\theta_B$ and thus the phase coefficient (φ_i) of $i-$th element

can be expressed by $\varphi_i = -ikd\sin\theta_B$ [23], [24]. As a consequence, $F(\theta)$ can be expressed by

$$F(\theta) = \sum_{i=0}^{N-1} a_i \exp\left(ji\left(\frac{2\pi}{\lambda}d\sin\theta - \frac{2\pi}{\lambda}d\sin\theta_B\right)\right) = \sum_{i=0}^{N-1} a_i \exp\left(ji\left(\frac{2\pi}{\lambda}d\sin\theta - \Delta\phi_B\right)\right). \quad (2)$$

It is clear that modification of the complex excitations (a_i, φ_i) of the beamforming network can reconfigure the radiation pattern as desired. For a uniformly distributed PAA (i.e., $a_i = 1$), the amplitude pattern of the antenna array $|F(\theta)|$ is given by

$$|F(\theta)| = \frac{\sin\frac{N\pi}{\lambda}d(\sin\theta - \sin\theta_B)}{\sin\frac{\pi}{\lambda}d(\sin\theta - \sin\theta_B)} = \frac{\sin\frac{N}{2}\left(\frac{2\pi d}{\lambda}\sin\theta - \Delta\phi_B\right)}{\sin\frac{1}{2}\left(\frac{2\pi d}{\lambda}\sin\theta - \Delta\phi_B\right)}. \quad (3)$$

According to (3), the beam pointing/steering angle is determined by the following condition:

$$\frac{1}{2}\left(\frac{2\pi d}{\lambda}\sin\theta - \Delta\phi_B\right) = m\pi \quad (4)$$

where m is an integer. Usually, if $\Delta\phi_B$ is provided by electrical phase shifters, $m = 0$ is preferred to allow a low phase difference being constant for the interested RF wavelength/frequency range. The beam steering angle θ_B can be deduced into

$$\theta_B = \arcsin\left(\frac{\lambda}{2\pi d}\cdot\Delta\phi_B\right) \quad (5)$$

which becomes a function of λ according to (5), leading to beam squint phenomenon. Hence the traditional electrical beamformer suffers limited bandwidth.

In contrast, the photonic beamformer based on PTTD can overcome it since the phase difference between the adjacent PAA elements is given by

$$\Delta\phi_B = 2\pi f\Delta\tau_{PTTD} \quad (6)$$

where $f = c/\lambda$ is the RF frequency, c is the light velocity in vacuum, and $\Delta\tau_{PTTD}$ is the relative PTTD difference independent on λ or f. Consequently, the beam steering angle is given by

$$\theta_B = \arcsin\left(\frac{c}{d}\cdot\Delta\tau_{PTTD} + m\frac{\lambda}{d}\right) = \arcsin\left(\frac{n_{eff}\cdot\Delta L}{d} + m\frac{\lambda}{d}\right) \quad (7)$$

where ΔL is the fiber delay line difference corresponding to $\Delta\tau_{PTTD}$, and n_{eff} is the effective refractive index of the fiber delay line. The integer m in (7) is determined by the condition

$$\left|\frac{c}{d}\cdot\Delta\tau_{PTTD} + m\frac{\lambda}{d}\right| \le 1. \quad (8)$$

According to (7) and (8), any desired θ_B can be formed by proper design of PTTD network due to the periodic property of the trigonometric function in our photonic beam formers.

In order to illustrate the different impacts of electrical phase shifters and PTTD on PAA, we simulate the radiation patterns of 8, 10, and 12 GHz frequencies at X band by substituting (2) and (5) into (3). The spacing between adjacent antenna elements is set as a half of 12-GHz RF wavelength (i.e., $d = 0.0125$ m). Fig. 1(a) and (b) compares the radiation patterns at $\theta_B \approx 28.7^\circ$ and $N = 8$ when the phase difference between the electrical phase shifters is $\Delta\phi_B = 86.4^\circ$ and the time difference of the PTTD between different channels is $\Delta\tau_{PTTD} = 20$ ps, respectively. For electrical phase shifters, the direction of the main lobe increases as the RF

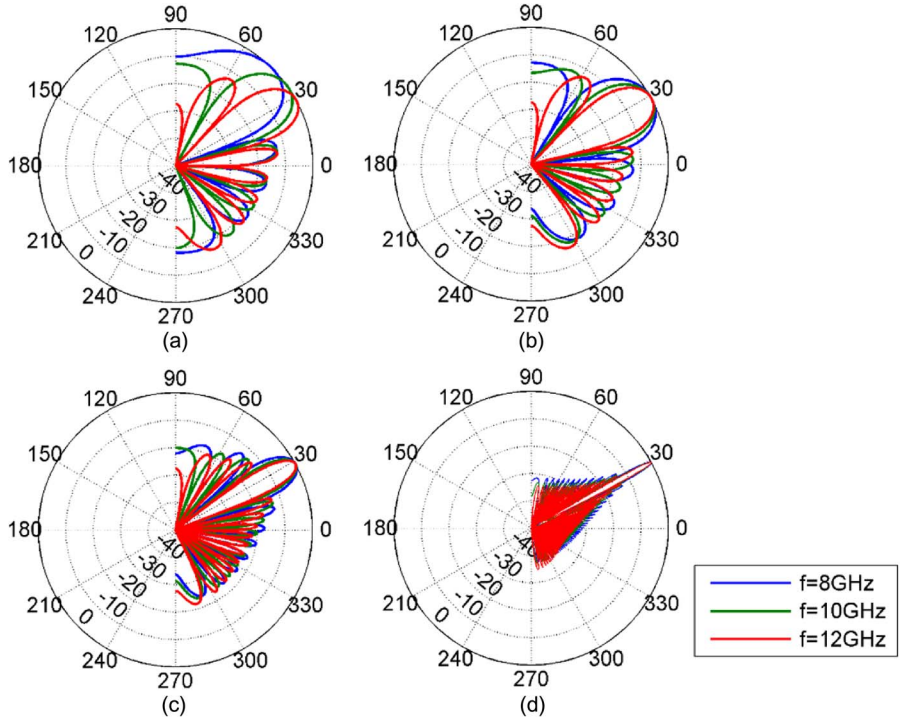

Fig. 1. Simulated radiation patterns of PAA at $\Delta\phi_B = 86.4^\circ$ or $\Delta\tau_{PTTD} = 20$ *ps* (corresponding to a beam steering angle of $\theta_B \approx 28.7^\circ$) based on electrical phase shifters (a) or PTTD (b)–(d). The number of the antenna elements are (a) $N = 8$, (b) $N = 8$, (c) $N = 16$, and (d) $N = 73$ (the maximum channel number with 100-GHz spacing defined by ITU).

frequency decreases (see Fig. 1(a)), showing obvious beam squint phenomenon. For PTTD, however, the main lobe is free from the beam squint as shown in Fig. 1(b). Besides, as plotted in Fig. 1(c) and (d), the width of main lobe is apparently decreased when the antenna elements of PTTD are increased, resulting in better resolution.

3. System Configuration

The system configuration of the proposed multi-channel multi-bit programmable photonic beamformer is schematically shown in Fig. 2. Fig. 2(a) shows that a number of (such as M) multi-channel multi-bit programmable PTTD subnetworks are connected in parallel by a $1 \times$ M optical splitter. As depicted in Fig. 2(b), the multi-channels (such as N) in one PTTD subnetwork, corresponding to multi-channel PAA elements, are basically realized by cascading DWDMs on the ITU grid. The laser array, shared by all M parallel PTTD subnetworks (see Fig. 2(a) and (b)), provides separated optical carriers whose wavelengths are on the ITU grid as well. Thus, each optical carrier together with the related channel of the cascaded DWDMs determines one channel of the PTTD subnetwork. A Mach-Zehnder $LiNbO_3$ electro-optic modulator (EOM) biased at in-quadrature point is applied to modulate the input RF subcarrier to all the optical carriers combined by the front-end DWDM. The modulated light wave is amplified by an erbium-doped fiber amplifier (EDFA) to compensate the insertion loss of the photonic devices, such as the EOM, $1 \times$ M optical splitter, etc. The amplified light wave passes towards M parallel PTTD subnetworks to accomplish wavelength-controlled multi-channel operation of true-time delays (TTDs). The light wave is de-multiplexed by the back-end DWDM in each PTTD subnetwork to multi-channel spatially-separated optical carriers, which are converted to electrical signals by a photodetector (PD) array and fed to N pieces of PAA elements.

The details of one programmable multi-bit PTTD subnetwork based on cascaded DWDMs is realized by use of multiple stages of wavelength-controlled multi-channel TTD. As shown in

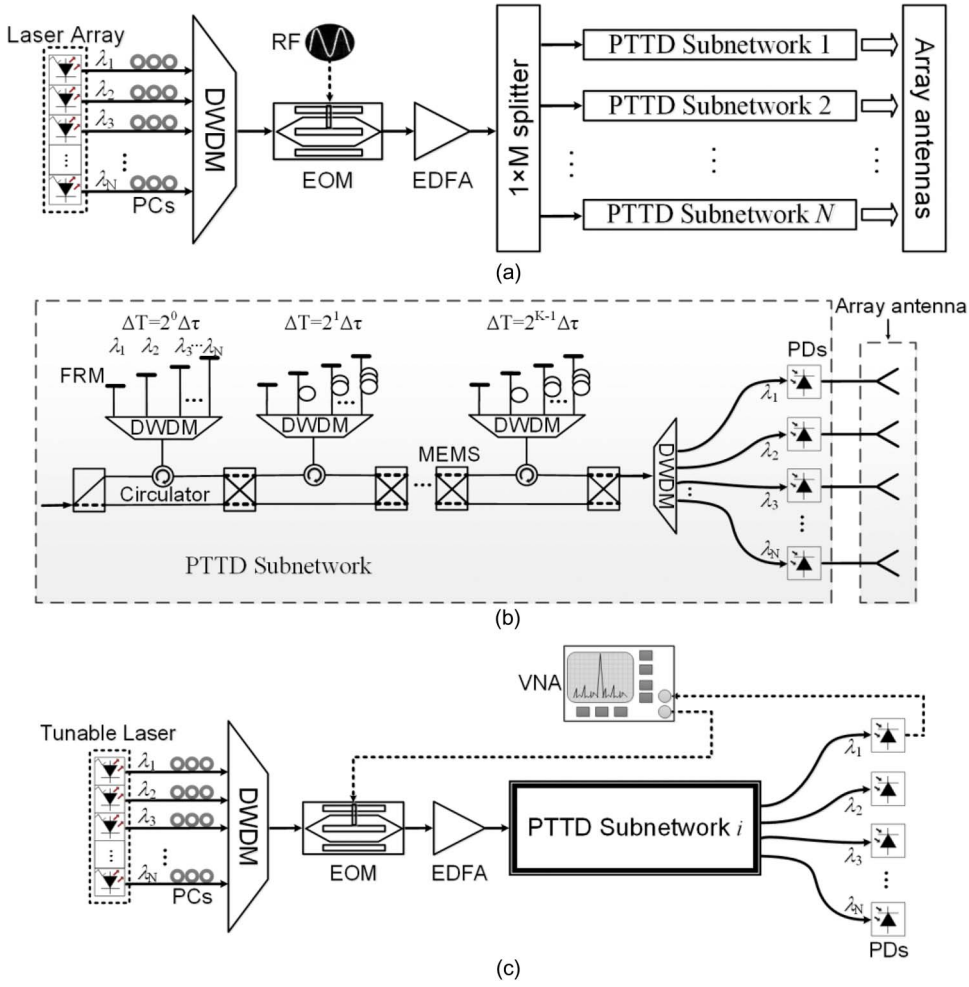

Fig. 2. Schematic of multi-channel multi-bit programmable photonic beamformer. (a) M parallel PTTD subnetworks. (b) One PTTD subnetwork. (c) Characterization of PTTD subnetwork based on a VNA.

Fig. 2(b), each stage incorporates two states (i.e., "0" and "1"), performing one-bit TTD operation. The "0" state is a segment of fiber, providing an equal TTD for all channels. The "1" state provides an incremental TTD for signals of different wavelengths, which is realized by a TTD unit consisting of a circulator, a multi-port DWDM, multiple FRMs and N segments of fibers with an equal TTD difference. The neighboring stages are connected by 2×2 MEMS optical switches with two status (bar or cross) for different bits of TTD operation. The input modulated light is routed to the common port of the DWDM via the circulator and de-multiplexed to the related channel depending on its wavelength. As mentioned, each channel has different TTD provided by the high-precision tailored fibers. The multi-channel light wave is reflected back towards the DWDM common port by FRMs where they are combined together and sent to the next stage. FRMs are used to eliminate the influence of fiber birefringence [25]. It is noted that, for RF signals, all stages of the PTTD subnetwork are free from dispersion effect due to the nature of optical fiber transmission capacity. The port 1 of each DWDM serves as the reference. For the first-stage (the first bit), the round-trip fiber length increment between neighboring channels is set to be ΔL. In order to linearly scan the steering angle, the fiber-length increment of the K_{th}-stage DWDM equals $2^{K-1}\Delta L$. Accordingly, the TTD increment of K_{th}-stage stages

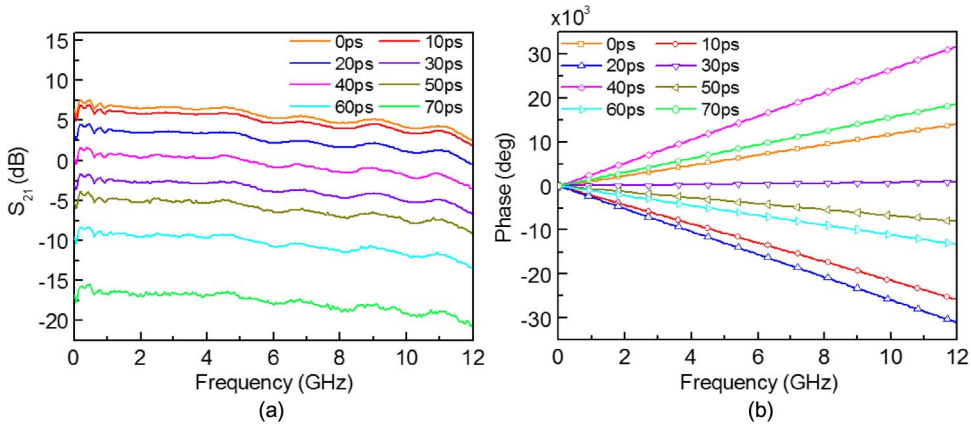

Fig. 3. Measured amplitude (a) and unwrapped phase. (b) Dependence on RF frequency for 3-bit PTTD at $\lambda_1 = 1556.55$ nm. Phase slopes in (b) represents eight discrete TTDs.

become $2^{K-1}\Delta\tau$ with $\Delta\tau = n_{eff} \cdot \Delta L/c$. By simultaneously controlling the MEMS driver circuit, the status of all the MEMS optical switches can be effectively programmed and thus 2^K discrete time differences between adjacent antenna elements can be achieved, i.e., K-bit operation in one PTTD subnetwork can be performed.

In consequence, an architecture of PTTD network with M parallel PTTD subnetworks with N channels and K bits can be topologically configured out for PAA with a large number of elements $(M \times N)$. The architecture of the photonic beamformer has several obvious advantages. Thanks to the optical summation principle [26], the wavelength division multiplexing technology is coherent in RF domain but incoherent in photonic domain, allowing a high dynamic range [7]. In order to change dynamically the beam direction of the radiation patterns of PAA, the PTTD network can be reconfigured by programming a control circuit of optical switches. The time response is on the order of millisecond level mainly limited by the MEMS optical switches. It can simultaneously provide a large range of TTD (determined by the number of stages) and a high resolution of TTD (determined by the fiber increment ΔL). Moreover, the number of multiple spatially-separated channels is fairly large due to the commercial availability of telecom optical demultiplexers (DWDM), which enables a narrow width of main lobe and high beamforming resolution (see Fig. 1(c) and (d)).

4. Experiment and Results

A proof-of-concept experiment of the programmable photonic beamformer is implemented using a four-channel 3-bit PTTD subnetwork of 3-stage cascaded DWDMs. There are 16 ports in each thin-film DWDM (channels 10–40 on the ITU grid) with 200-GHz frequency spacing from 1545.32 nm to 1569.59 nm. The narrow-linewidth laser array at hand has only four available channels covering C-band and L-band (Alnair Labs, TLG-200) with maximum output power of 15.5 dBm and measured RIN of less than -140 dB/Hz. In order to preliminarily demonstrate the multi-channel operation of the photonic beamformer, we set four wavelengths of the laser array at $\lambda_1 = 1556.55$ nm, $\lambda_2 = 1554.94$ nm, $\lambda_3 = 1553.33$ nm, $\lambda_4 = 1551.72$ nm, corresponding to ITU channels of CH26, CH28, CH30, CH32 in DWDMs, respectively. The polarization states of all channels are optimized by polarization controllers (PCs). The insertion loss and electro-optical bandwidth of the EOM (Photline, MX-LN-20) are 2.7 dB and 20 GHz, respectively. The EDFA is used to compensate for the insertion loss of the EOM and the PTTD subnetwork (about 33 dB). The PDs have a bandwidth of 16 GHz and a responsivity of 0.7 A/W. The length difference (ΔL) of the tailored fiber segments is precisely measured to be 2 mm [20], [21], and 3-bit (or eight) TTDs are estimated to be $\Delta\tau_{PTTD} = 0$, 10, 20, 30, 40, 50, 60, and 70 ps, respectively.

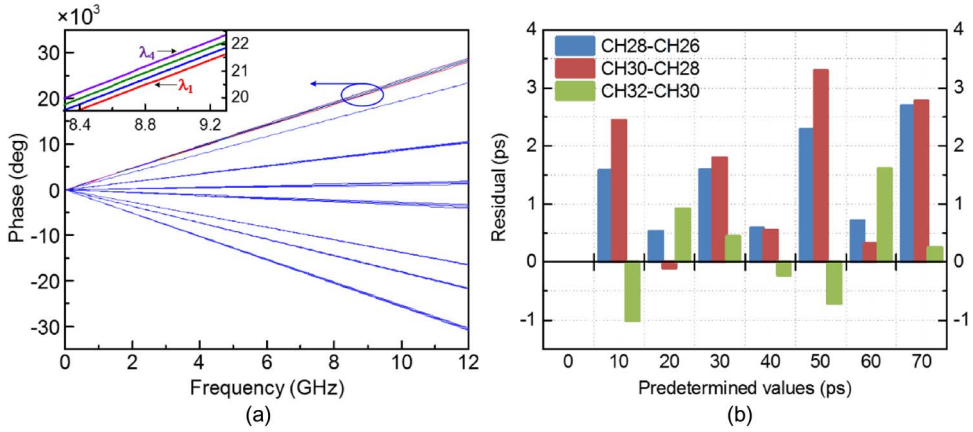

Fig. 4. (a) Comparison of unwrapped phase dependence on RF frequency for four channels. Each channel comprises eight TTDs, while the CH26 serves as a reference. (b) Residuals of relative TTD difference between adjacent ports of the DWDM.

An RF vector network analyzer (VNA, Agilent PNA-X Network analyzer N5247A) is used to characterize the RF transfer function of the photonic beamformer, which is depicted in Fig. 2(c). The RF output of the analyzer replaces the RF source at the electric input of the EOM, while its input is connected to the output of the PD of each channel to be measured. Note that the RF analyzer between its input and output RF ports is beforehand calibrated to cancel out all the distortions apart from the system under test. The forward transmission coefficient S_{21} is measured for all 4 channels within a RF range from 10 MHz to 12 GHz. As an example, Fig. 3 plots the amplitude $S_{21}(f)$ and unwrapped RF phase $(\angle S_{21}(f))$ as a function of the RF frequency for CH26 $(\lambda_1 = 1556.55\ \text{nm})$ under different TTDs. As can be seen in Fig. 3(a), the amplitude $S_{21}(f)$ for each TTD decreases slightly because of the RF responses of EOM and PD. Note that there is a certain periodic ripple in Fig. 3(a), which originates from the impedance mismatch between the RF input of the EOM $(\sim 40\ \Omega)$ and the RF cable of the VNA (50 Ω). Besides, it decreases gradually when the value of TTD increases (i.e., more DWDM stages included). Nonetheless, the photonic beamformer presented above has a flat power response for all channels since all channels go through the same optical and electrical components at a specific TTD and the cascaded DWDMs have excellent RF characteristics [16], [17]. According to the repeatability test, the amplitude ripples (or fluctuations) of all channels for each TTD is always less than 1 dB. It must be noted that such amplitude ripples mainly originate from the uncertain connection/insertion loss among all passive elements (like MEMS optical switches, FRMs, and connectors). The uncertain insertion loss of even more connectors for PAA with a large number of elements could be further reduced by fiber splicing, which will be implemented in our future study. Fig. 3(b) shows that the unwrapped phase shift of each TTD has an approximate linear relation on the RF frequency, leading to the frequency-independent phase shift and straightforwardly verifying the proposed photonic beamformer having no beam squint.

The same experimental investigation is conducted to characterize the delay properties of all the 32 RF links of the photonic beamformer, comprising four channels with 3-bit TTDs per channel. The results are compared in Fig. 4(a), where $\angle S_{21}(f)$ of CH26 $(\lambda_1 = 1556.55\ \text{nm})$ for each TTD always serve as the reference for the other three channels (CH28, CH30 and CH32). Note that the selection of the reference channel (CH26) is not unique because the photonic beamformer is only determined by the relative TTD differences between neighboring channels (see Eq. (7)). It is clearly shown that a tiny difference does exist among four channels in each group (see the inset of Fig. 4(a)), which accounts for the incremental TTD between adjacent channels. The TTDs are calculated by the derivative $(1/360^\circ)d(\angle S_{21}(f))/df$ with $\angle S_{21}(f)$ in degrees and f in GHz, and the relative TTD difference between neighboring channels are evaluated by subtraction.

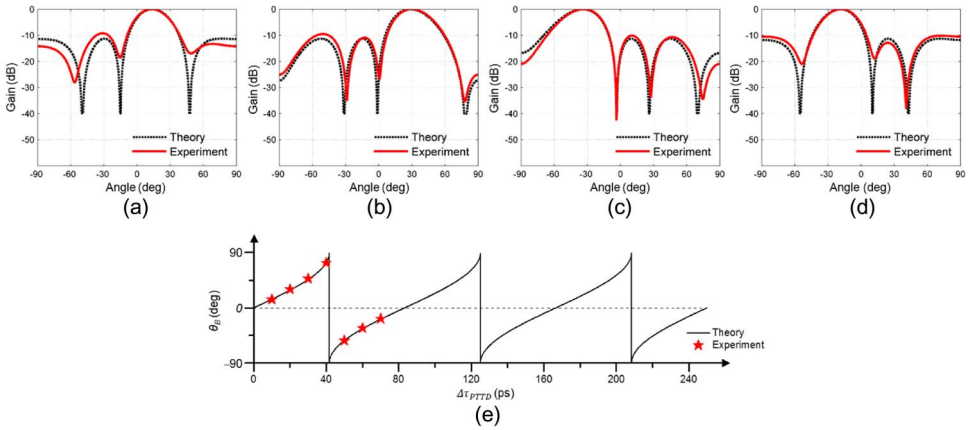

Fig. 5. PAA radiation patterns based on photonic beamformer when the relative TTD difference of the PTTD subnetwork is (a) 10 ps, (b) 20 ps, (c) 60 ps, or (d) 70 ps, corresponding to the steering angle of the main lobe of 13.1°, 29.9°, −33.2° and −17.9°, respectively. The dashed and solid curves represent the theoretical analysis and experimental results, respectively. (e) Steering angle as a function of the relative TTD difference of the PTTD subnetwork. Solid pentangles: experimental data; solid curve: theoretical analysis.

TABLE 1

Comparison between theoretical and experimental PAA radiation patterns for all relative TTD differences when the amplitude and/or phase ripples are considered

Delay (ps)	Steering Angle (°)				3dB Bandwidth (°)			
	Theory	Amplitude and Phase Ripples	Amplitude Ripples	Phase Ripples	Theory	Amplitude and Phase Ripples	Amplitude Ripples	Phase Ripples
10	13.9	13.1	13.9	13.1	27.2	27.6	27.6	27.1
20	28.7	29.9	28.7	29.9	30.4	30.1	29.8	30.9
30	46.1	47.2	46.1	47.3	41.9	42.1	40.4	43.8
40	73.7	73.0	73.7	73.0	78.5	77.4	78.5	77.4
50	-53.1	-53.5	-53.1	-53.6	68.5	70.3	69.9	69.0
60	-34.1	-33.2	-34.1	-33.2	32.6	31.5	31.9	32.2
70	-18.7	-17.9	-18.7	-17.9	27.9	28.3	28.3	27.8

As illustrated in Fig. 4(b), there are absolute deviations (or residuals), which is responsible for the phase ripples, less than 3.5 ps comparing to the predetermined values. The small deviation in each group is possibly due to the precise fiber cutting errors (±0.35 mm, i.e., ±3.5 ps) in replicating the fiber-length delays among the identical DWDM (Fig. 2). The connection among all passive components by connectors has ignorable impact on the phase ripples because the TTD fabrication (i.e., fiber cutting) and characterization were performed after normal connection of components. Note that if the fiber splicing of all passive components is further implemented, the TTD fabrication and characterization will be more flexible.

Finally, we compare and analyze the PAA radiation patterns based on the experimental results and theoretical analysis when $N = 4$ and $d = 0.0125$ m at $f = 12$ GHz, which are shown in Fig. 5(a)–(d). Note that the random phase ripples with peak-to-peak of 3.5 ps and random amplitude ripples with peak-to-peak of 1 dB among four channels are considered in the experimental results. All the main lobes of the experimental radiation patterns steered to the desired angles (see Fig. 5(e)). As long as the relative TTD difference $\Delta\tau_{PTTD}$ is larger than about 42 ps or its integer multiples, the steering angle will be folded back into $[-90°, 90°]$ as determined by Eq. (7). For instance, 13.1° for 10 ps while −17.9° for 70 ps. The influence of the phase and/or amplitude ripples on the PAA radiation patterns (including steering angles and 3 dB bandwidth) are summarized in Table 1. There are some differences of the side lobes (also at their notches) between the experimental and theoretical results, which are mainly caused by the small phase

ripples (~3.5 ps) and small amplitude ripples (~1 dB) between adjacent channels. Taken into account the important figures of merit for PAA system (the steering angle, 3 dB bandwidth of the main lobe and average side lobe level) [3], it is worth noting that the small phase and amplitude ripples have negligible influence (see Table 1). Such little influence can be further reduced to a large extent when more channels in cascaded DWDMs are adopted into the photonic beamformer (see Fig. 1(c) and (d)).

5. Conclusion

A novel multi-channel multi-bit programmable photonic beamformer, having a capacity of high-resolution and large range of the TTD, based on cascaded DWDMs with multiple channels was proposed and demonstrated. The *N*-channel *K*-bit PPTD subnetwork can be easily extended into parallel architecture for PAA with a large number of elements by use of an optical splitter. Different TTDs in one PTTD subnetwork can be obtained by programmable control of the status of MEMS optical switches. With the increase of the stages of the DWDM, more bits operation to achieve larger TTDs can be realized. A preliminary experiment demonstrates that the main lobe of the radiation pattern steers accurately to the desired directions and the impact of small phase ripples introduced by fiber-cutting and amplitude ripples among multiple channels is negligible. Since all components involved in this study are commercially available and mature in telecom or fiber-optic industry, more channels and bits beamformer can be practically implemented. Besides, thanks to the periodic property of the trigonometric function in our photonic beamformer, as long as the entire TTD in one PPTD subnetwork or *M* parallel PTTD networks are extended, a large range of the steering angles for PAA with a large number of elements can be formed. Although the proof-of-concept preliminary experiment is still bulky with large size, it is highly expectable to adopt the novel photonic beamformer as an advantageous candidate for the applications in wideband radar and wireless communications if silicon photonic integration is developed [27]–[29]. Besides, through the material compensation [30] or structure optimization [31], athermal silicon photonic devices can be potentially free from the heating problem. Moreover, the maximum RF signal may go beyond X band towards Ku-Ka bands by replacing the EOM and PDs with 40-GHz or larger bandwidth.

References

[1] R. Tang and R. W. Burns, "Array technology," *Proc. IEEE*, vol. 80, no. 1, pp. 173–182, Jan. 1992.
[2] L. C. Godara, "Application of antenna arrays to mobile communications, Part II: Beam-forming and direction-of-arrival considerations," *Proc. IEEE*, vol. 85, no. 8, pp. 1195–1245, Aug.1997.
[3] M. Skolnik, *Radar Handbook*, 3rd ed. New York, NY, USA: McGraw-Hill, 2008.
[4] H. Zmuda and E. N. Toughlian, *Photonic Aspects of Modern Radar*, Boston, MA, USA: Artech House, 1994.
[5] J. Capmany, B. Ortega, and D. Pastor, "A tutorial on microwave photonic filters," *J. Lightw. Technol.*, vol. 24, no. 1, pp. 201–229, Jan. 2006.
[6] J. Yao, "Microwave photonics," *J. Lightw. Technol.*, vol. 27, no. 3, pp. 314–335, Feb. 2009.
[7] S. Blanc, M. Alouini, K. Garenaux, M. Queguiner, and T. Merlet, "Optical multibeamforming network based on WDM and dispersion fiber in receive mode," *IEEE Trans. Microw. Theory Tech.*, vol. 54, no. 1, pp. 402–411, Jan. 2006.
[8] M. Y. Chen, "Hybrid photonic true-time delay modules for quasi-continuous steering of 2-D phased-array antennas," *J. Lightw. Technol.*, vol. 31, no. 6, pp. 910–917, Mar. 2013.
[9] P. Wu, S. Tang, and D. E. Raible, "A prototype high-speed optically-steered X-band phased array antenna," *Opt. Exp.*, vol. 21, no. 26, pp. 32 599–32 604, Dec. 2013.
[10] H. Zmuda, R. A. Soref, P. Payson, S. Johns, and E. N. Toughlian, "Photonic beamformer for phased array antennas using a fiber grating prism," *IEEE Photon. Technol. Lett.*, vol. 9, no. 2, pp. 241–243, Feb. 1997.
[11] C. Fan *et al.*, "Compact high frequency true-time-delay beamformer using bidirectional reflectance of the fiber gratings," *Opt. Fiber Technol.*, vol. 19, no. 1, pp. 60–65, Jan. 2013.
[12] J.-D. Shin, B.-S. Lee, andB.-G. Kim, "Optical true time-delay feeder for X-band phased array antennas composed of 2 × 2 optical MEMS switches and fiber delay lines," *IEEE Photon. Technol. Lett.*, vol. 16, no. 5, pp. 1364–1366, May 2004.
[13] T. Akiyama *et al.*, "Spatial light modulator based optically controlled beamformer for variable multiple-spot beam antenna," in *Proc. Int. Top. Meet. Microw. Photon. Conf.*, 2011, pp. 401–404.
[14] Y. Zhang, H. Wu, D. Zhu, and S. Pan, "An optically controlled phased array antenna based on single sideband polarization modulation," *Opt. Exp.*, vol. 22, no. 4, pp. 3761–3765, Feb. 2014.

[15] M. Burla *et al.*, "System integration and radiation pattern measurements of a phased array antenna employing an integrated photonic beamformer for radio astronomy applications," *Appl. Opt.*, vol. 51, no. 7, pp. 789–802, Mar. 2012.
[16] O. Raz, R. Rotman, and M. Tur, "Wavelength-controlled photonic true time delay for wide-band applications," *IEEE Photon. Technol. Lett.*, vol. 17, no. 5, pp. 1076–1078, May 2005.
[17] O. Raz, S. Barzilay, R. Rotman, and M. Tur, "Submicrosecond scan-angle switching photonic beamformer with flat RF response in the C and X bands," *J. Lightw. Technol.*, vol. 26, no. 15, pp. 2774–2781, Aug. 2008.
[18] L. Yaron, R. Rotman, S. Zach, and M. Tur, "Photonic beamformer receiver with multiple beam capabilities," *IEEE Photon. Technol. Lett.*, vol. 22, no. 23, pp. 1723–1725, Dec. 2010.
[19] Y. Han and B. Jalali, "Photonic time-stretched analog-to-digital converter: Fundamental concepts and practical considerations," *J. Lightw. Technol.*, vol. 21, no. 12, pp. 3085–3103, Dec. 2003.
[20] H. Lee, H. Jeon, and J. W. Jung, "Optical true time-delay beam-forming for phased array antenna using a dispersion compensating fiber and a multi-wavelength laser," in *Proc. 4th Annu. Caneus, FBW*, 2011, pp. 1–4.
[21] S. Li *et al.*, "High-resolution measurement of fiber length change with optical low-coherence reflectometer based on a fiber-ring structure," *Appl. Phys. Exp.*, vol. 4, no. 6, pp. 062501-1–062501-3, Jun. 2011.
[22] S. Li, X. Li, W. Zou, and J. Chen, "Rangeability extension of fiber-optic low-coherence measurement based on cascaded multistage fiber delay line," *Appl. Opt.*, vol. 51, no. 6, pp. 771–775, Feb. 2012.
[23] R. C. Johnson and H. Jasik, *Antenna Engineering Handbook*. New York, NY, USA: McGraw-Hill, 1984.
[24] R. E. Collin, *Antennas and Radiowave Propagation*. New York, NY, USA: McGraw-Hill, 1985.
[25] X. Li, L. Peng, S. Wang, Y.-C. Kim, and J. Chen, "A novel kind of programmable 3n feed-forward optical fiber true delay line based on SOA," *Opt. Exp.*, vol. 15, no. 25, pp. 16 760–16 766, Dec. 2007.
[26] T. Merlet *et al.*, "Photonics for RF signal processing in radar systems," in *Proc. IEEE Int. Top. Meet. Microw. Photon.*, 2004, pp. 305–308.
[27] F. Xia, L. Sekaric, and Y. Vlasov, "Ultracompact optical buffers on a silicon chip," *Nat. Photon.*, vol. 1, no. 1, pp. 65–71, Dec. 2006.
[28] J. Xie *et al.*, "Continuously tunable reflective-type optical delay lines using microring resonators," *Opt. Exp.*, vol. 22, no. 1, pp. 817–823, Jan. 2014.
[29] P. A. Morton, J. B. Khurgin, Z. Mizrahi, and S. J. Morton, "Commercially packaged optical true-time-delay devices with record delays of wide bandwidth signals," presented at the *CLEO—Applications Technol. Conf.*, San Jose, CA, USA, 2014, Paper AW3P.6.
[30] L. Zhou, K. Okamoto, and S. J. B. Yoo, "Athermalizing and trimming of slotted silicon microring resonators with UV-sensitive PMMA upper-cladding," *IEEE Photon. Technol. Lett.*, vol. 21, no. 17, pp. 1175–1177, Jun. 2009.
[31] L. Lu *et al.*, "CMOS-compatible temperature-independent tunable silicon optical lattice filters," *Opt. Exp.*, vol. 21, no. 8, pp. 9447–9456, Apr. 2013.